

Structural, electronic, and optical properties of ZrO_2 from *ab initio* calculations

J. C. Garcia, L. M. R. Scolfaro

*Instituto de Física, Universidade de São Paulo,
CP 66318, 05315-970 São Paulo, SP, Brazil*

A. T. Lino

*Instituto de Física, Universidade Federal de Uberlândia,
CP 593, 38400-902 Uberlândia, MG, Brazil*

V. N. Freire, G. A. Farias

*Departamento de Física, Universidade Federal do Ceará,
CP6030, 60455-900 Fortaleza, CE, Brazil*

C. C. Silva, H. W. Leite Alves

*Departamento de Ciências Naturais,
Universidade Federal de São João del Rei,
CP110, 36301-160 São João del Rei, MG, Brazil*

S. C. P. Rodrigues, E. F. da Silva Jr.

Departamento de Física, Universidade Federal de Pernambuco, 50670-901 Recife, PE, Brazil

(Dated: September 28, 2006)

Abstract

Structural, electronic, and optical properties for the cubic, tetragonal, and monoclinic crystalline phases of ZrO_2 , as derived from *ab initio* full-relativistic calculations, are presented. The electronic structure calculations were carried out by means of the all-electron full potential linear augmented plane wave method, within the framework of the density functional theory and the local density approximation. The calculated carrier effective masses are shown to be highly anisotropic. The results obtained for the real and imaginary parts of the dielectric function, the reflectivity, and the refraction index, show good agreement with the available experimental results. In order to obtain the static dielectric constant of ZrO_2 , we added to the electronic part, the optical phonons contribution, which leads to values of $\epsilon_1(0) \simeq 29.5, 26.2, 21.9$, respectively along the xx, yy , and zz directions, for the monoclinic phase, in excellent accordance with experiment. Relativistic effects, including the spin-orbit interaction, are demonstrated to be important for a better evaluation of the effective mass values, and in the detailed structure of the frequency dependent complex dielectric function.

I. INTRODUCTION

Zirconia (ZrO_2) is a material of great technological potential importance due to its outstanding mechanical and electrical properties, high dielectric constant and wide band gap. Among the ZrO_2 applications, are: its use as gas sensors, solid fuel cells, high durability coating, catalytic agents, etc. In recent years, its gap ($E_g \sim 6$ eV) and dielectric properties ($\epsilon \sim 25$) suggested its potential to replace SiO_2 in advanced metal oxide semiconductor devices (MOS) in gate stack, dynamic access memory devices, and optical applications [1–5]. Moreover, it has a large band-offset in direct contact with Si and good thermal stability. These attracting properties has led zirconia based oxides to be widely studied in recent years [6–8].

ZrO_2 presents polymorphism with monoclinic, tetragonal, and cubic phases. The monoclinic phase (m- ZrO_2) of undoped ZrO_2 is thermodynamically stable at temperatures below 1170°C . The tetragonal phase structure (t- ZrO_2) arises when heating ZrO_2 , being stable between 1170°C and 2370°C , as well as above this; through its melting point (2706°C), the cubic phase (c- ZrO_2) is then observed. The temperature in which the tetragonal to cubic transformation occurs can be lowered, by the addition of solutes such as MgO , CaO , Y_2O_3 , allowing the achievement of the stabilized c-phase even at room temperature.

Previous investigations of ZrO_2 , based on first-principles electronic structure calculations, have been reported in the literature [9–16]. Most of them dealt with the structural and electronic properties of ZrO_2 , in its cubic, tetragonal, and monoclinic phases [9–13, 15]. The zirconia optical properties, or more specifically its complex dielectric function has been addressed by French *et al* (electronic frequency regime only) by carrying out *ab initio* electronic structure calculations via the orthogonalized linear-combination-of-atomic-orbitals method [16], and more recently, by Zhao and Vanderbilt [14] and by Rignanese *et al* [17], by means of *ab initio* pseudopotential calculations. However, in the work of Ref.[17] only the ZrO_2 cubic and tetragonal structural phases have been considered, while in that of Ref.[14], although in the work all three phases (cubic, tetragonal, and monoclinic) are studied, only the lattice contributions to the dielectric tensor have been addressed so far. Moreover, in these studies, relativistic effects including the spin-orbit interaction were not taken into account in the calculations, neither have been provided values for the ZrO_2 carrier effective masses, which are fundamental to model the tunnelling currents through floating gate memory devices that

use, e.g., ZrO_2 as the tunnelling oxide.

In this work, we present results of state-of-the-art first-principles calculations for the structural, electronic, and optical properties of ZrO_2 in its monoclinic, tetragonal, and cubic phases. From the band structures, the ZrO_2 conduction- and valence-band effective masses have been obtained, in the most important symmetry axis of the Brillouin zone. The full-relativistic effects, properly taken into account in the calculations, are demonstrated to be relevant for a more precise evaluation of its electron- and hole-effective-mass values, as well as in the detailed structure of the electronic contribution to its frequency dependent dielectric function, $(\epsilon^{elect}(w))$. As a consequence of the role played by the inclusion of full-relativistic effects in the calculations, the obtained changes in the reflectivity spectrum and refraction index are also significant.

In order to realistically obtain the value for the static dielectric constant $\epsilon_1(0)$, we also calculated the lattice contributions, mostly arising from the transverse optical phonon modes, to the low-frequency dielectric function, for the different phases. The resulting calculated static dielectric constant for m- ZrO_2 is in excellent agreement with the values reported in the literature. Moreover, the results obtained for the reflectivity and refraction index for its monoclinic phase are in good accordance with the available experimental data.

II. CALCULATION DETAILS

The electronic structure calculations were carried out using the density-functional theory in the local-density approach (DFT-LDA) by means of the *ab initio* full-potential self-consistent linear augmented plane wave (FLAPW) method (Wien2k code [18]). The generalized gradient approximation (GGA) was adopted for the exchange-correlation potential [19]. A similar approach has been recently applied to study the structural, electronic, and optical properties of cubic SrTiO_3 and HfO_2 [20, 21]. The Zirconium 4s-, 4p-, 4d-, and 5s, and the Oxygen 2s, 2p electrons were treated as part of the valence states. The cutoff angular momentum was $l = 10$ for wave functions, and $l = 5$ for charge densities and potentials inside the spheres. Muffin-tin sphere radii were assumed equal for both Zr and O. The number of symmetrized \mathbf{k} -points, used as input for the self-consistent charge density determination, was 47, 75, and 100- \mathbf{k} points in the irreducible symmetry wedge of the BZ, respectively for the cubic, tetragonal, and monoclinic phases. The value $RKMAX = 9$ was

adopted for the three different phases. With these assumptions, the energy bands were converged within 10^{-5} eV, and the total energy within 10^{-6} eV. The core electron states were treated full-relativistically, whereas the valence states were treated both, non-relativistic and full-relativistically, i.e. including the spin-orbit interaction, besides the Darwin and mass-velocity corrections.

In addition, we have also used the DFT-LDA, with the plane-wave description of the wavefunctions, and the pseudopotential method (*Abinit* code [22]) for the evaluation of the phonon contributions to the real part of the dielectric function ($\varepsilon_1^{latt}(w)$), as will be discussed later. With this approach, we are able to unveil and estimate the total value of the static dielectric constant of ZrO_2 in the form $\varepsilon_1(0) = \varepsilon_1^{elect}(0) + \varepsilon_1^{latt}(0)$, for the three phases cubic, tetragonal, and monoclinic.

III. RESULTS AND DISCUSSIONS

A. Structural properties

The cubic ZrO_2 phase (c- ZrO_2) belongs to the space group $Fm\bar{3}m$ with crystalline structure of fluorite, i.e. face-centered cubic lattice with three atoms at the basis, being one Zr atom at the position (0,0,0) and the oxygen atoms at the position (1/4, 1/4, 1/4), for which the BZ is the usual 14-faces polyhedra. We have obtained through a total energy minimization process, a lattice constant value of the cubic phase $a = 5.139$ Å, slightly larger than that calculated by Králik *et al* [12], using the pseudopotential method and the local density approximation (LDA), and closer to the experimental value of 5.09 Å [13]. The value obtained by us confirms that the GGA approximation leads to lattice constant values which are slightly overestimated in relation to the experimental value.

The tetragonal phase (t- ZrO_2) is described by the $P4_2/nmc$ group. As shown by Zhao and Vanderbilt [14], the t- ZrO_2 phase is obtained from the cubic one, by properly performing alternate displacements Δc of the oxygen atoms in the cubic structure. Our optimization process consisted in minimizing the total energy and forces, until "converged" Δc , c , and a values have been reached. The obtained values were $a = 5.10$ Å, $c = 5.23$ Å, and the internal parameter $d_z = \Delta c/c = 0.05$, close to the experimental ones [13] ($a = 5.05$ Å, $c = 5.18$ Å, and $d_z = 0.0574$), as well as close to the theoretical values reported by Králik *at al.* [12]

($a = 5.04 \text{ \AA}$ and $c = 5.10 \text{ \AA}$ and $d_z = 0.0423$).

For the monoclinic phase, which is described by the $P21/c$ group, we have evaluated the total energy for several lattice constant values, in order to have a good description of the equilibrium properties for the bulk m-ZrO₂, in which case, for sake of reducing computational time, we use the *Abinit* code [22]. The results were fitted by the Murnaghan equation of state, and we have obtained, for the monoclinic structure, $a = 5.12 \text{ \AA}$, $b = 5.16 \text{ \AA}$, $c = 5.33 \text{ \AA}$, and $\theta = 99.6$ degrees. These results are in accordance with the available experimental [13] ($a = 5.15 \text{ \AA}$, $b = 5.21 \text{ \AA}$, $c = 5.31 \text{ \AA}$, and $\theta = 99.23$ degrees), and theoretical results [15] ($a = 5.20 \text{ \AA}$, $b = 5.25 \text{ \AA}$, $c = 5.41 \text{ \AA}$, and $\theta = 99.60$ degrees). We have used the later ones in the band structure calculations performed with Wien2k code, as well as to calculate effective mass values and optical properties for the monoclinic phase.

B. Electronic properties

Table I presents the band gap energies, together with the valence-to-conduction band transition symmetry, for all three phases of ZrO₂. For the cubic phase, the band gap is indirect at $X \rightarrow \Gamma$, with an energy of 3.09 eV when a non-relativistic calculation is considered, and with energy of 3.30 eV, if the calculations are performed by taking into account the full relativistic effects, i.e. the scalar-relativistic and spin-orbit effects. The direct band gap, at Γ , is of 3.61 (3.80) eV within a non-relativistic (full-relativistic) calculation. Our values for the band gaps are very close to those obtained by Králik *et al.* [12], in which a pseudopotential LDA method was used. We recall that, the theoretical values for the band gap energy are smaller when compared with the experimental one, due to the well-known underestimation of conduction band states energies in *ab initio* calculations which are performed within DFT. Experimental values, as reported by French *et al.* [16], are found in the range of 6.1 to 7.08 eV.

Due to the spin-orbit interaction, we observe a spin-orbit (so) splitting energy of the valence band top (v), at the Γ -point, which for the cubic phase is $\Delta_{so}^v(\Gamma) = 69 \text{ meV}$. There are no experimental data for Δ_{so} in ZrO₂ reported so far.

For the tetragonal phase, the energy transitions at $X \rightarrow \Gamma$, $Z \rightarrow \Gamma$, and $\Gamma \rightarrow \Gamma$ are very near. An indirect gap of 3.80 (4.01) eV, and a direct one of ~ 3.9 (~ 4.1) eV, were obtained from non-relativistic (full-relativistic) calculations. A value of $\Delta_{so}^v(\Gamma) = 9 \text{ meV}$

has been observed for the spin-orbit splitting energy of the valence band top, at Γ , for t-ZrO₂. The band gap energy values, obtained through the full-relativistic calculations, are well compared with those obtained by Králik *et al.* [12]. The experimental values for t-ZrO₂ lie in the range of 5.8 to 6.6 eV, according to the results reported by French *et al.* [16].

For the monoclinic phase, we have obtained an indirect gap of ~ 3.4 eV (~ 3.6) eV in a non-relativistic (full-relativistic) calculation, and a direct band gap of 3.50 eV (3.64) eV, so much close to the value of the indirect one, that it is difficult to assure whether the gap is direct or indirect. As one goes from the cubic to tetragonal, and then to the monoclinic structural phase, the symmetry lowering is responsible for the removal of the degeneracy, hence to the appearance of so many energy bands in the monoclinic case.

Figure 1 shows the non-relativistic results obtained for the band structure, along high symmetry directions of the BZ, and the total density of states (TDOS) for the three phases of ZrO₂. The *main* character of the peaks in the TDOS is also emphasized. The results for band structures, as obtained from the full-relativistic calculations are presented in Fig. 2. In the upper valence part of the band structure, the O(2p)-related states are predominant, while in its lower part, the O(2s)- derived states are the most relevant, independently of inclusion of the relativistic corrections, for all three phases. The Zr(4p) states appear rather deep in the valence band (-26 eV) and, due to the spin-orbit coupling are split into a group at -26 and a group at -28 eV, corresponding to $j=3/2$ and $j=1/2$ manifolds, respectively.

C. Carrier effective masses

The valence- and conduction-band effective masses for the cubic, tetragonal, and monoclinic phases of ZrO₂, at relevant symmetry points of the BZ, are presented in Table II for several directions. Full- and non-relativistic (see the values in parenthesis) results are shown. In order to remain within the region of validity of the parabolic approximation, the effective masses were calculated by considering the energy curves within a small region of radius 0.5% centered on the extremum of interest.

As we observe, in both the valence and conduction bands, the carrier effective masses are very anisotropic, i.e., show a relevant dependence on the \vec{k} direction. Moreover, remarkable differences arise when the relativistic effects are taken into account. In particular, for the cubic phase, relativistic effects are seen to be most important in the $\Gamma - X$ direction, for

holes and electrons, while these effects are more relevant in the $\Gamma - Z$ direction, for the case of holes, for the tetragonal phase, and in the $\Gamma - Y$ direction, for electrons and holes, for the monoclinic phase. So far, there are no reported experimental data in the literature of carrier effective masses in ZrO_2 . This represents the first report of effective mass values, as calculated for all phases of ZrO_2 , of fundamental importance to the modelling of advanced devices based on this oxide.

D. Optical properties

The electronic contributions to the real ($\varepsilon_1(\omega)$) and imaginary ($\varepsilon_2(\omega)$) parts of the complex dielectric function, $\varepsilon(\omega) = \varepsilon_1(\omega) + i\varepsilon_2(\omega)$, can be obtained from the band structure directly through the Wien2k code [18], ε_1 from ε_2 , and vice-versa, using the Kramers-Kronig relations [23]. Once is known the imaginary part $\varepsilon_2(\omega)$, from the FLAPW electronic structure calculations, the real part $\varepsilon_1(\omega)$ is then given by [23]

$$\varepsilon_1(\omega) = 1 + (2/\pi) \int_0^\infty d\omega' \frac{\omega'^2 \varepsilon_2(\omega')}{\omega'^2 - \omega^2}. \quad (1)$$

Other optical properties, such as the reflectivity $R(\omega)$ and the complex refraction index $n(\omega)$ can also be obtained. We took into account that energy gaps are under evaluated by DFT [19], by adopting the following procedure: the dielectric function, and all the related optical properties, were obtained by performing an upward rigid shift, to the experimental energy value of the band gap [16], of all the conduction band states. In general, for metals and conductor materials, the optical properties calculations demand a great number of eigenvalues and eigenvectors, therefore, a study of convergence, that considers the number of k-points used, is necessary. In the case of the insulating oxide ZrO_2 studied here, we have verified that no more than about 100 symmetrized k-points were sufficient.

Figure 3 shows the imaginary part of the dielectric function (electronic contribution), for the three phases of ZrO_2 , considering energies till 30 eV. For the cubic phase, all the diagonal components of ε_2 are identical ($\varepsilon_{xx} = \varepsilon_{yy} = \varepsilon_{zz}$), whereas the off-diagonal components are zero. The energy spectrum was *adjusted* by shifting it upwards, to the band gap experimental value for the monoclinic phase, $E_g = 5.83$ eV [16]. For tetragonal and monoclinic phases, the adjustment was taken by considering the same experimental value as for the monoclinic

phase, once this later is the observed phase at ambient temperature. The function ε_2 , for t-ZrO₂, has all off-diagonal components equal to zero, but symmetry assures that $\varepsilon_{xx} = \varepsilon_{yy} \neq \varepsilon_{zz}$. For the monoclinic phase, the components that are different from zero are ε_{xx} , ε_{yy} , ε_{zz} , and ε_{xz} .

In order to avoid confusion, results for both full-relativistic (frel) and non-relativistic (nrel) calculations are shown in Fig.3 only for the cubic phase. Relative changes in the values of the dielectric function, due to relativistic effects amount to 5%, at maximum, for all cases. For the tetragonal and monoclinic phases, the presented results derive from full-relativistic calculations. A comparison of the theoretical findings with the experimental result of Camagni *et al.* [24], as derived from reflectivity data, shows better agreement for the monoclinic phase for which two more pronounced peaks occur in the theoretical curve, at 7.5 eV and ~ 11.5 eV.

The real part of the complex dielectric function, ε_1 , is presented in Fig. 4, for the three phases of ZrO₂. As for the case of ε_2 (shown in Fig.3), we show results for ε_1 as obtained from full-relativistic and non-relativistic calculations only for c-ZrO₂; for the other two phases, tetragonal and monoclinic, the results depicted in parts (b) and (c) of Fig.4 correspond to full-relativistic calculations.

In order to compare the theoretical result with experiment, we show in Fig.5 the calculated xx -component of the real part of the dielectric function, ε_{1xx} , for m-ZrO₂, till energies of 30 eV, together with the data reported by Camagni *et al.* [24] for two samples of m-ZrO₂ stabilized with 12% and 24% of Yttria. Excellent accordance is seen between theory and experiment.

In Fig. 6, we show the calculated reflectivity (R) for the three phases of ZrO₂, together with the experimental results, as extracted from French *et al.* [16] and from Camagni *et al.* [24]. In the former work, the authors have considered three different samples of ZrO₂, in cubic, tetragonal, and monoclinic phases. These experimental results are referred as Exp.[2] in Fig.6. The data in the figure, referred as Exp.[1], correspond to m-ZrO₂ single crystals stabilized with 12% of Yttria [24]. Again, a good agreement between theoretical and experimental results is observed for the monoclinic phase.

Figure 7 shows the behavior of the refraction index, as function of energy, for all three phases of ZrO₂, as derived from full-relativistic calculations. For the cubic phase, we also included the result obtained from a non-relativistic calculation, for comparison. In Table III

are depicted the values of the refraction index, at two different energies, for the tetragonal phase. They compare well with the data reported by French *et al.*, as obtained from VUV spectroscopy measurements [16].

E. Phonon Contribution to the Dielectric Function

In order to realistically describe the dielectric function and, in particular, to evaluate the static dielectric constant, $\varepsilon_1(0)$, we have also to consider the phonon contribution to the low-frequency region of the frequency-dependent dielectric function. The enhancement, observed in the measured values of the ZrO_2 dielectric constant, is due to the role played by the optical phonons. We have used the *Abinit* code [22] to unveil this phonon contribution to the dielectric functions of the three phases. With this program, we calculated the equations of state, the phonon frequencies and eigendisplacements for the structures (not shown in this work). In this case, we adopted the Troullier-Martins pseudopotentials in the calculations [25], and the phonon dynamics were obtained by means of the adiabatic perturbation density functional theory. According to the available data, and previous theoretical results, for the phonon frequencies [14], our results are in complete agreement.

From the obtained results, we have calculated the frequency dependence of the real part of the dielectric constant (as described by Rignanese *et al.* [17] and Gonze *et al.* [26]) for the monoclinic, tetragonal, and cubic phases.

In Fig. 8 we show the results for $\varepsilon_1^{(latt)}(\omega)$, for m- ZrO_2 , along the x , y , and z axis, together with a fitting by means of the Lorentz-Drude model, i.e.

$$\varepsilon_1^{(latt)}(\omega) = \sum_{i=1}^n \frac{\omega_{pi}^2(\omega_{TOi}^2 - \omega^2)}{[(\omega_{TOi}^2 - \omega^2)^2 + \gamma_i^2\omega^2]}, \quad (2)$$

where n is the total number of oscillators, each one with the transversal optical (TO) phonon frequency ω_{TOi} , ω_{pi} is the plasmon frequency for the i^{th} oscillator, and γ_i is its damping parameter, which is directly related to sample size. The Drude-Lorentz curves are a guide for the eye, and show that our calculated data follow this model. In the case of the x -component of $\varepsilon_1^{(latt)}(\omega)$, we included four oscillators, and the obtaining fitting parameters were $\omega_{p1} = 541.83 \text{ cm}^{-1}$ and $\gamma_1 = 0.05 \text{ cm}^{-1}$ for the TO mode at 709 cm^{-1} , $\omega_{p2} = 635.54 \text{ cm}^{-1}$ and $\gamma_2 = 0.05 \text{ cm}^{-1}$ for the TO mode at 485.1 cm^{-1} , $\omega_{p3} = 1052.34 \text{ cm}^{-1}$ and $\gamma_3 = 0.05 \text{ cm}^{-1}$ for the TO mode at 316 cm^{-1} , and $\omega_{p4} = 493.07 \text{ cm}^{-1}$ and $\gamma_4 = 0.05 \text{ cm}^{-1}$ for

the TO mode at 220 cm^{-1} .

To describe the frequency dependence of the dielectric constant parallel to the y axis, given by the Lorentz-Drude model, we needed five oscillators. The obtained fitting parameters were $\omega_{p1} = 517.81 \text{ cm}^{-1}$ and $\gamma_1 = 0.05 \text{ cm}^{-1}$ for the TO oscillator at 576 cm^{-1} , $\omega_{p2} = 493.44 \text{ cm}^{-1}$ and $\gamma_2 = 0.05 \text{ cm}^{-1}$ for the TO oscillator at 473 cm^{-1} , $\omega_{p3} = 997.54 \text{ cm}^{-1}$ and $\gamma_3 = 0.05 \text{ cm}^{-1}$ for the TO oscillator at 413 cm^{-1} , $\omega_{p4} = 576.96 \text{ cm}^{-1}$ and $\gamma_4 = 0.05 \text{ cm}^{-1}$ for the TO oscillator at 354 cm^{-1} , and $\omega_{p5} = 465.39 \text{ cm}^{-1}$ and $\gamma_5 = 0.05 \text{ cm}^{-1}$ for the TO oscillator at 247 cm^{-1} .

Finally, we have also to include five oscillators, in order to describe the frequency dependence of the dielectric constant parallel to the z axis. The obtained fitting parameters were $\omega_{p1} = 147.44 \text{ cm}^{-1}$ and $\gamma_1 = 1.22 \text{ cm}^{-1}$ for the TO mode at 485.1 cm^{-1} , $\omega_{p2} = 353.93 \text{ cm}^{-1}$ and $\gamma_2 = 0.81 \text{ cm}^{-1}$ for the TO mode at 399 cm^{-1} , $\omega_{p3} = 1029.0 \text{ cm}^{-1}$ and $\gamma_3 = 2.18 \text{ cm}^{-1}$ for the TO mode at 354 cm^{-1} , $\omega_{p4} = 513.52 \text{ cm}^{-1}$ and $\gamma_4 = 11.1 \text{ cm}^{-1}$ for the TO mode at 316 cm^{-1} , and $\omega_{p5} = 327.06 \text{ cm}^{-1}$ and $\gamma_5 = 0.0001 \text{ cm}^{-1}$ for the TO mode at 220 cm^{-1} .

The calculated static dielectric tensor, due to lattice contribution, for the monoclinic phase of ZrO_2 is

$$\begin{pmatrix} 24.12 & 0 & 1.77 \\ 0 & 21.20 & 0 \\ 1.77 & 0 & 17.02 \end{pmatrix}. \quad (3)$$

Therefore, using $\varepsilon_1(0) = \varepsilon_1^{(electr)}(0) + \varepsilon_1^{(latt)}(0)$, and using the $\varepsilon_1^{(electr)}(0)$ from Figure 4(c) we get

$$\begin{pmatrix} 29.52 & 0 & 1.83 \\ 0 & 26.20 & 0 \\ 1.83 & 0 & 21.92 \end{pmatrix}. \quad (4)$$

The average value of the static dielectric constant, for the monoclinic phase, is then given by $\bar{\varepsilon}_1(0) \sim 25.9$, which agrees fairly well with reported experimental values of ~ 25 [Ref.[2]].

It is worth mentioning that, we have also evaluated the dielectric constants for t- and m- ZrO_2 , by using the same approach described above. The calculated phonon contribution for the tetragonal phase, added to the corresponding electronic part, lead to an average value of the static dielectric constant of $\bar{\varepsilon}_1(0) = 55.8$, a value which is as high as that obtained

for the cubic phase, 44.4. Details of these calculations will be published elsewhere [27]. These findings are another indication that the measured dielectric constant for the ZrO_2 is correctly described by considering the oxide in its monoclinic phase.

IV. CONCLUSIONS

We have performed an extended study, based on *ab initio* calculations, of the structural, electronic, and optical properties for the cubic, tetragonal, and monoclinic crystalline phases of ZrO_2 , which takes into account scalar relativistic and spin-orbit contributions to the electronic structure, as well as the phonon contributions to the low-frequency regime of the dielectric function. For the band structure calculations, we used the DFT-GGA approach by means of the FLAPW method. Due to the spin-orbit interaction, we observe a spin-orbit (so) splitting energy of the top of the valence band (v) at the Γ -point, which for the cubic phase is $\Delta_{so}^v(\Gamma) = 69$ meV, while for the tetragonal phase is $\Delta_{so}^v(\Gamma) = 9$ meV. So far, there are no experimental data reported for Δ_{so} in ZrO_2 .

The carrier effective masses are shown to be highly anisotropic, with the relativistic corrections playing an important role; this is of special interest when modelling advanced ZrO_2 -based devices. In addition we report, with the relativistic corrections, an evaluation of a spin-orbit effective mass in the valence band, as well as the heavy- and light-hole (electron) effective masses at the valence (conduction) band, in particular for cubic ZrO_2 .

The results obtained for the real and imaginary parts of the dielectric function, for the reflectivity, and for the refraction index, show good agreement with the available experimental results. In order to obtain the static dielectric constant of ZrO_2 , we added to the electronic part, the optical phonons contribution, which leads to values of $\varepsilon_1(0) \simeq 29.5, 26.2, 21.9$, along the xx, yy , and zz directions, respectively, for the monoclinic phase, in excellent accordance with experiment.

Relativistic effects, taking also into account the spin-orbit interaction, are demonstrated to be important for a better evaluation of the effective mass values, and in the detailed structure of the frequency dependent complex dielectric function. We were able to unveil and estimate a more realistic total value of the static dielectric constant of ZrO_2 , in the form $\varepsilon_1(0) = \varepsilon_1^{elect}(0) + \varepsilon_1^{latt}(0)$, yielding an average value of ~ 25.9 , in good agreement with reported experimental values of ~ 25 .

Acknowledgments

We acknowledge support from the Brazilian funding agencies, CNPq, FAPESP, and FAPEMIG. One of the authors, SCPR, would like to acknowledge the scholarship from the project CT-ENERG/CNPq (Grant No. 503.570/03-6).

-
- [1] The International Roadmap for Semiconductor 2004, ([url:http://public.itrs.net](http://public.itrs.net)).
 - [2] G. D. Wilk, R. M. Wallace, and J. M. Anthony, J. Appl. Phys. **89**, 5243 (2001).
 - [3] M. Houssa, V. V. Afanašev, A. Stesmans, and M. M. Heyns, Appl. Phys. Lett. **77**, 1885 (2000).
 - [4] S. J. Wang, C. K. Ong, S. Y. Xu, P. Chen, W. C. Tiju, J. W. Chai, A. C. H. Huan, W. J. Yoo, J. S. Lim, W. Feng, and W. K. Choi, Appl. Phys. Lett. **78**, 1604 (2001).
 - [5] Y. -S. Lin, R. Puthenkovilakam, J. P. Chang, C. Bouldin, I. Levin, N. V. Nguyen, J. Ehrstein, Y. Sun, P. Pianetta, T. Conard, W. Vandervorst, V. Venturo, and S. Selbrede, J. Appl. Phys. **93**, 5945 (2003).
 - [6] J. -P. Maria, D. Wicaksana, A. I. Kingon, B. Busch, H. Schulte, E. Garfunkel, and T. Gustafsson, J. Appl. Phys. **90**, 3476 (2001).
 - [7] G. D. Wilk, R. M. Wallace, and J. M. Anthony, J. Appl. Phys. **87**, 484 (2000).
 - [8] C. J. Först, C. R. Ashman, K. Schwarz, and P. E. Blöchl, Nature **427**, 53 (2003).
 - [9] J. E. Lowther, J. K. Dewhurst, J. M. Leger, and J. Haines, Phys. Rev. B **60**, 14485 (1999).
 - [10] R. Orlando, C. Pisani, C. Roetti, and E. Stefanovich, Phys. Rev. B **45**, 592 (1992).
 - [11] H. J. F. Jansen, Phys. Rev. B **43**, 7267 (1991).
 - [12] B. Králik, E. K. Chang, and S. G. Louie, Phys. Rev. B **57**, 7027(1998).
 - [13] E. V. Stefanovich, A. Shluger, and C. R. Catlow, Phys. Rev. B **49**, 11560(1994).
 - [14] X. Zhao and D. Vanderbilt, Phys. Rev. B **65**, 75105 (2002), and references therein.
 - [15] E. J. Walter, S. P. Lewis, A. M. Rappe, Surface Science **495**, 44(2001).
 - [16] R. H. French, S. J. Glass, F. S. Ohuchi, Y.-N. Xu, and W.Y. Ching, Phys. Rev. B **49**, 5133 (1994).
 - [17] G.-M. Rignanese, et al., *Phys. Rev. B* **69**, 184301 (2004).
 - [18] P. Blaha, K. Schwarz, G. Madsen, D. Kvasnicka, and J. Luitz, WIEN 2k, *Augmented Plane Wave + Local Orbitals Program for Calculating Crystal Properties*, Vienna, Austria, 2001. (See also <http://www.wien2k.at>).
 - [19] J. P. Perdew, K. Burke, and M. Ernzerhof, Phys. Rev. Lett. **77**, 3865 (1996).
 - [20] M. Marques, L. K. Teles, V. Anjos, L. M. R. Scolfaro, J. R. Leite, V. N. Freire, G. A. Farias, and E. F. da Silva Jr., Appl. Phys. Lett. **82**, 3074 (2003).

- [21] J. C. Garcia, L. M. R. Scolfaro, J. R. Leite, A. T. Lino, V. N. Freire, G. A. Farias, and E. F. da Silva Jr., *Appl. Phys. Lett.* **85**, 5022 (2004).
- [22] X. Gonze, et. al., *Comput. Mater. Sci.* **25**, 478 (2002), and references therein.
- [23] P. Y. Yu and M. Cardona, *Fundamentals of Semiconductors*, Springer-Verlag, Berlin (1996).
- [24] P. Camagni, G. Samoggia and L. Sangaletti, *Phys. Rev. B* **50**, 4292 (1994).
- [25] M. Fuchs and M. Scheffler, *Comput. Phys. Commun.* **119**, 67 (1999).
- [26] X. Gonze, and C. Lee, *Phys. Rev. B* **55**, 10355 (1997).
- [27] C. C. Silva and H. W. Leite Alves, *private communication*.

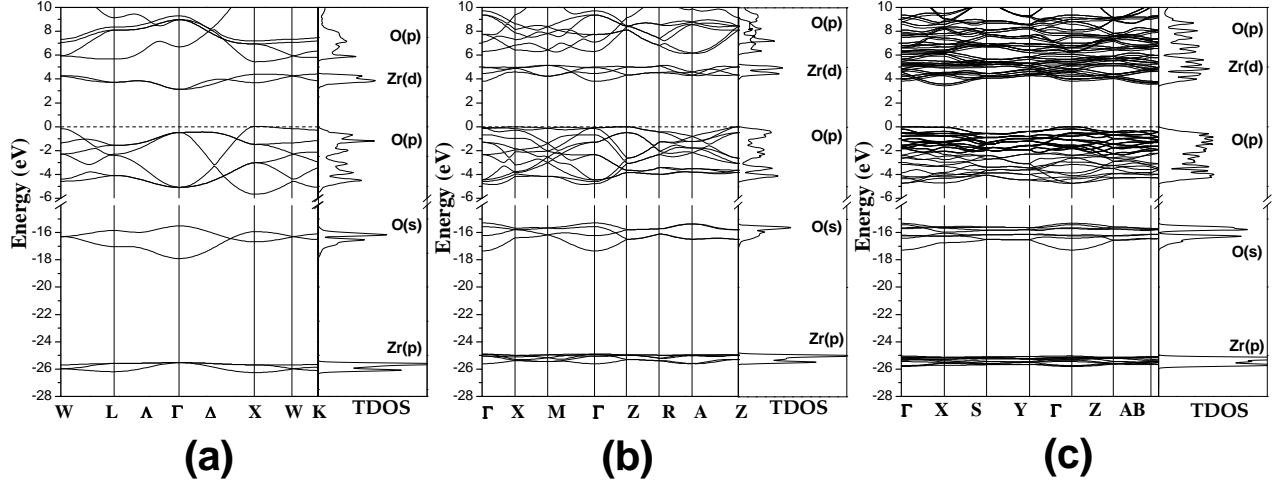


Figure 1

FIG. 1: Band structures, along high symmetry axis of the BZ, and total density of states (TDOS) for (a) cubic, (b) tetragonal, and (c) monoclinic phases of ZrO_2 , as obtained from non-relativistic calculations. The energy zero was taken at the valence band maximum, shown by a dashed horizontal line. The main character of the peaks in the TDOS is emphasized.

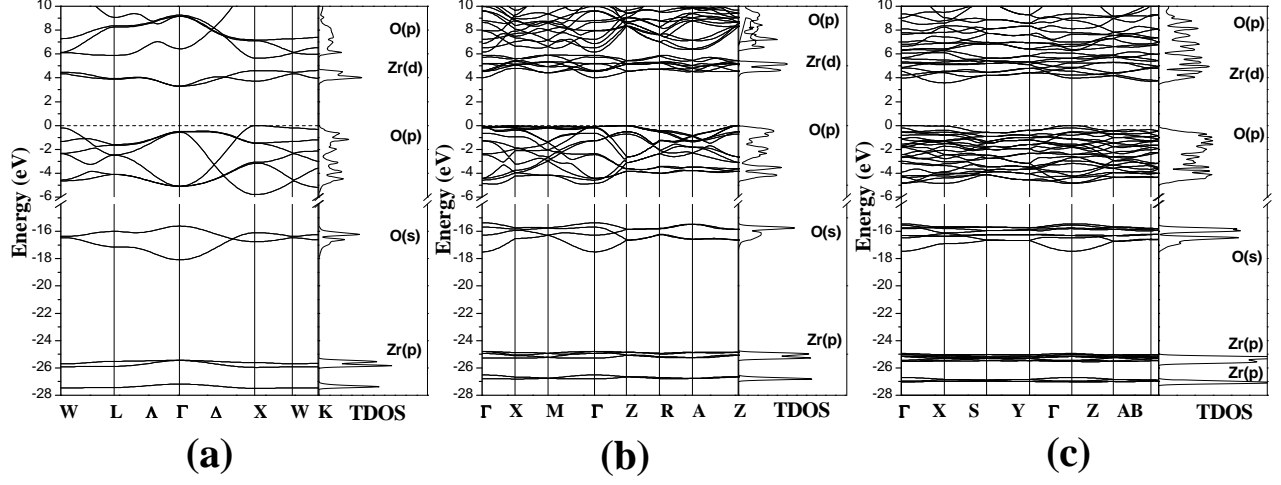


Figure 2

FIG. 2: Band structures, along high symmetry axis of the BZ, and total density of states (TDOS) for (a) cubic, (b) tetragonal, and (c) monoclinic phases of ZrO_2 , as obtained from full-relativistic calculations. The energy zero was taken at the valence band maximum, shown by a dashed horizontal line. The main character of the peaks in the TDOS is emphasized.

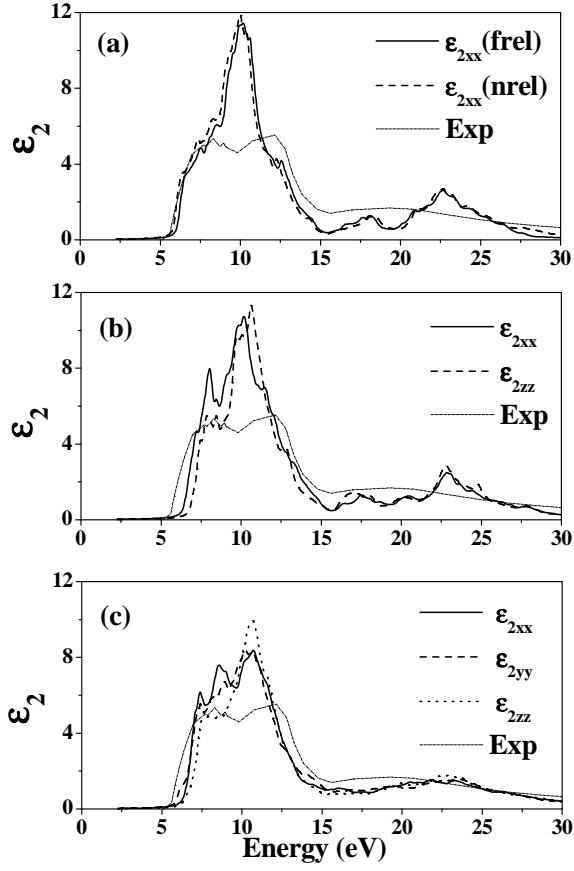


Figure 3

FIG. 3: Imaginary part of the dielectric function, ϵ_2 , versus energy, for the (a) cubic, (b) tetragonal, and (c) monoclinic phases of ZrO_2 , as obtained from full-relativistic calculations. Only in (a), results as obtained from full-relativistic calculations (*frel*) and non-relativistic calculations (*nrel*) are shown, for comparison. The theoretical curves were adjusted by performing a rigid shift upwards in energy to the experimental gap value for the monoclinic phase $E_g^{exp} = 5.83$ eV [Ref. [16]].

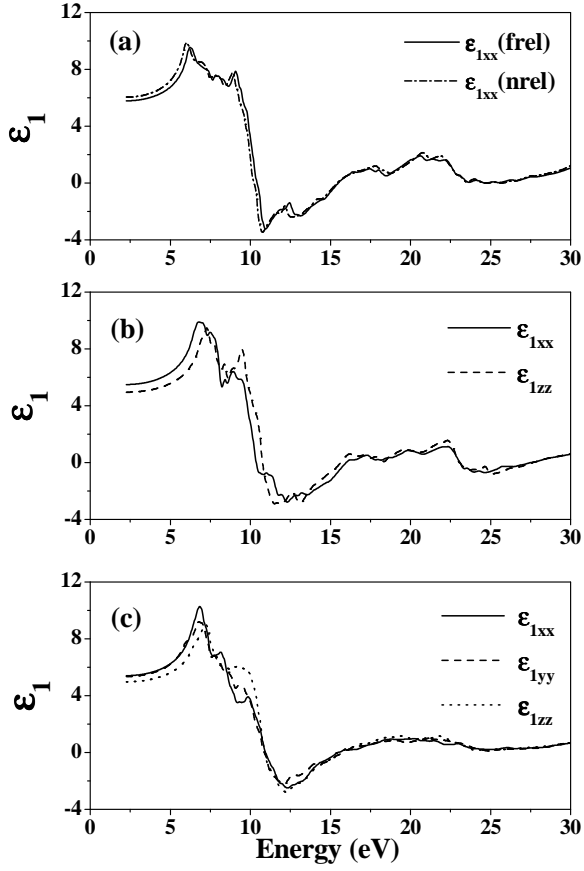


Figure 4

FIG. 4: Real part of the dielectric function, ϵ_1 , versus energy, for the (a) cubic, (b) tetragonal, and (c) monoclinic phases of ZrO_2 , as obtained from full-relativistic calculations. Only in (a), results as obtained from full-relativistic calculations (*frel*) and non-relativistic calculations (*nrel*) are shown, for comparison. The theoretical curves were adjusted by performing a rigid shift upwards in energy to the experimental gap value for the monoclinic phase $E_g^{exp} = 5.83$ eV [Ref. [16]].

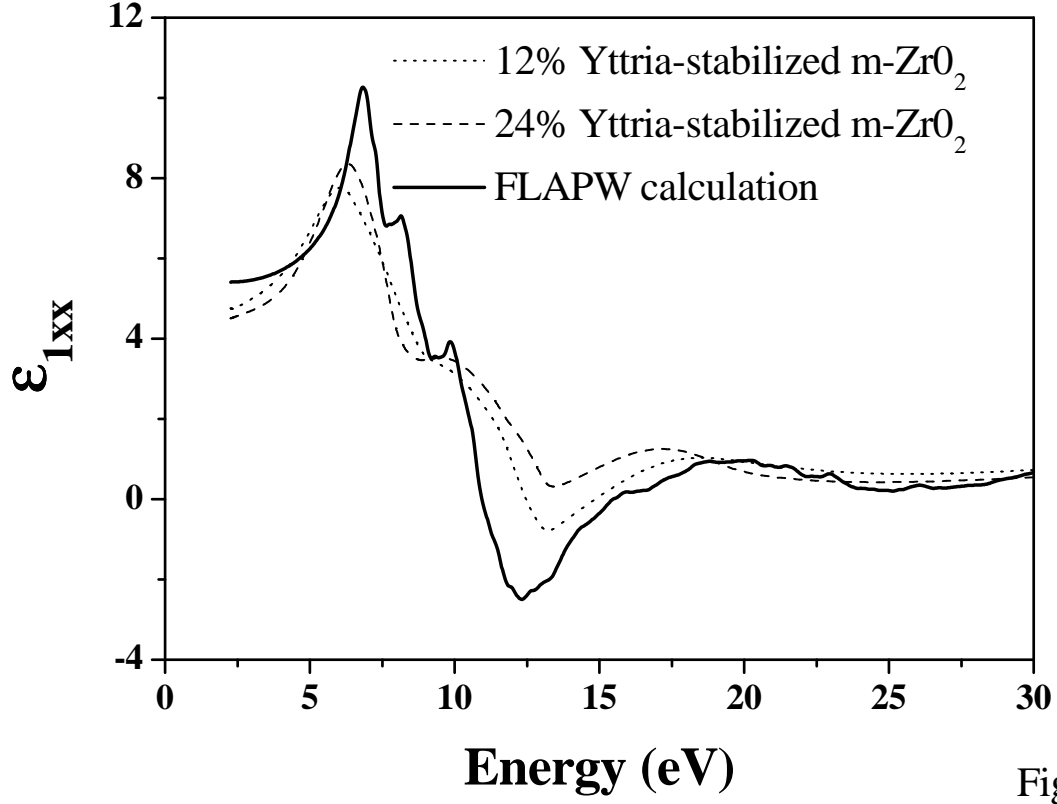


FIG. 5: xx -component of the real part of the dielectric function, ε_{1xx} , for monoclinic ZrO_2 , as obtained from full-relativistic FLAPW calculations, together with the experimental results as derived from reflectivity data, extracted from Ref.[24] for two yttria-stabilized samples.

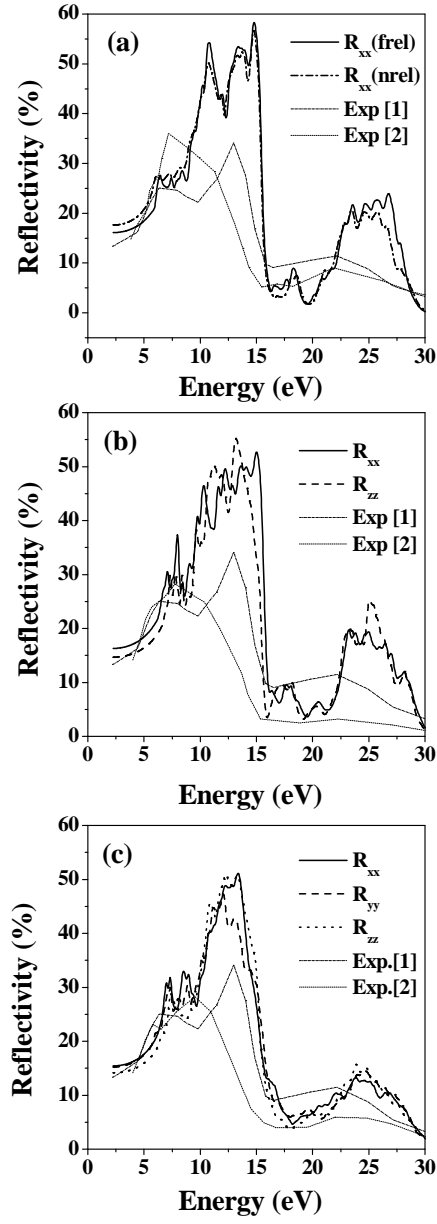


Figure 6

FIG. 6: Reflectivity (in %) versus energy, for the (a) cubic, (b) tetragonal, and (c) monoclinic phases of ZrO_2 , as obtained from full-relativistic calculations. Only in (a), results as obtained from full-relativistic calculations (*frel*) and non-relativistic calculations (*nrel*) are shown, for comparison. Also shown are the experimental curves, as extracted from French *et al.* [16] (Exp.[1]) and from Camagni *et al.*[24] (Exp.[2]).

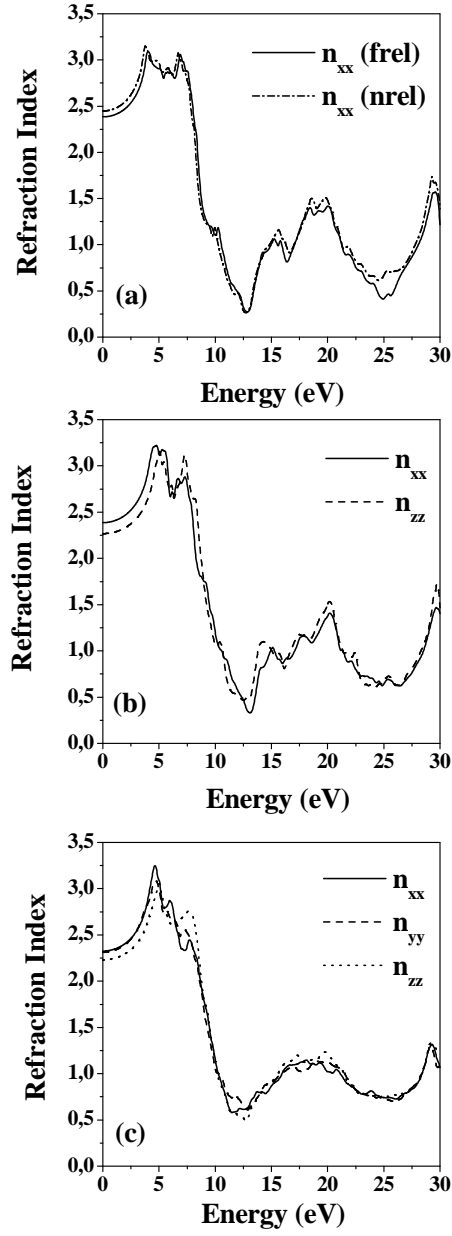


Figure 7

FIG. 7: Refraction index versus energy for the (a) cubic, (b) tetragonal, and (c) monoclinic phases of ZrO₂, as obtained from full-relativistic calculations. Only in (a), results as obtained from full-relativistic calculations (*frel*) and non-relativistic calculations (*nrel*) are shown, for comparison.

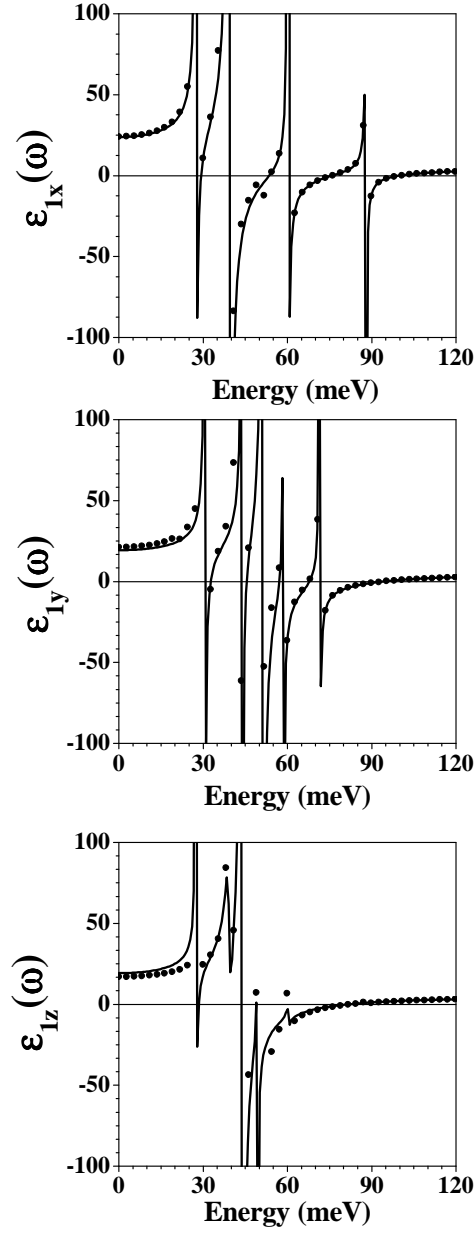


Figure 8

FIG. 8: Phonon contribution (full circles) to the low-frequency dependence of the real part of the dielectric function, $\epsilon_1^{latt}(\omega)$, as obtained from *ab initio* calculations, parallel to the x , y , and z axis, for monoclinic ZrO_2 . The solid line corresponds to a fitting by means of the Lorentz-Drude expression, and was used as a guide to the eye.

TABLE I: Band gap energies, E_g (in eV), and symmetry of the valence-to-conduction band transition, obtained from the non-relativistic (E_g^{nrel}) and full-relativistic (E_g^{frel}) calculations for the cubic, tetragonal, and monoclinic phases of ZrO_2 .

phase	valence-to-conduction band transition symmetry	E_g^{nrel}	E_g^{frel}
cubic	$X \longrightarrow \Gamma$	3.09	3.30
	$\Gamma \longrightarrow \Gamma$	3.61	3.80
	$X \longrightarrow X$	3.65	3.72
tetragonal	$Z \longrightarrow \Gamma$	3.80	4.01
	$X \longrightarrow \Gamma$	3.83	4.04
	$\Gamma \longrightarrow \Gamma$	3.88	4.09
monoclinic	$\Gamma \longrightarrow X$	3.44	3.58
	$\Gamma \longrightarrow \Gamma$	3.82	3.98
	$X \longrightarrow X$	3.50	3.64

TABLE II: Valence and conduction band effective masses (in units of the rest free electron mass, m_0), at relevant symmetry points of the BZ, for the cubic (c), tetragonal (t), and monoclinic (m) phases of ZrO_2 , as obtained from full-relativistic band structure calculations. In parenthesis, are shown the effective mass values as derived from non-relativistic calculations. m_h^* , m_e^* , m_{he}^* , m_{le}^* , m_{hh}^* , m_{lh}^* , and m_{so}^* stand for, respectively, hole, electron, heavy-electron, light-electron, heavy-hole, light-hole, and split-off hole effective masses.

phase	direction	valence	conduction
c	$\Gamma \longrightarrow L$	$m_{so}^* = 0.26; m_{lh}^* = 0.23(0.23); m_{hh}^* = 0.28(0.27)$	$m_{he}^* = 0.28(0.26); m_{le}^* = 0.27(0.26)$
	$\Gamma \longrightarrow X$	$m_{so}^* = 0.77; m_{lh}^* = 0.36(0.24); m_{hh}^* = 3.84(4.23)$	$m_{he}^* = 2.09(2.06); m_{le}^* = 0.51(0.48)$
	$X \longrightarrow \Gamma$	$m_h^* = 0.28(0.27)$	$m_e^* = 1.77(1.97)$
	$X \longrightarrow W$	$m_h^* = 3.38(3.29)$	$m_e^* = 1.17(1.33)$
t	$M \longrightarrow \Gamma$	$m_h^* = 0.47(0.47)$	$\dots(\dots)$
	$\Gamma \longrightarrow Z$	$m_h^* = 5.31(6.68)$	$m_e^* = 2.32(2.32)$
	$Z \longrightarrow R$	$m_h^* = 0.83 (0.88)$	$\dots (\dots)$
m	$X \longrightarrow \Gamma$	$\dots(\dots)$	$m_e^* = 1.16(1.12)$
	$X \longrightarrow S$	$m_h^* = 1.09(1.06)$	$m_e^* = 2.32(2.32)$
	$\Gamma \longrightarrow Y$	$m_h^* = 2.55(3.08)$	$m_e^* = 1.39(0.75)$
	$\Gamma \longrightarrow Z$	$m_h^* = 1.49(1.42)$	$m_e^* = 4.08(4.18)$

TABLE III: Values for the refraction index, at certain energies, as obtained from non-relativistic (n^{nrel}) and full-relativistic (n^{frel}) calculations, for tetragonal ZrO_2 . For comparison, the experimental results as observed from VUV spectroscopy measurements, and extracted from Ref. [16], are shown in the last column ($n_{exp.}$). n_{xx} and n_{zz} stand, respectively, for perpendicular and parallel refraction index to the axis along c , one of the lattice constants in the tetragonal lattice.

Energy (eV)	n_{xx}^{nrel}	n_{xx}^{frel}	n_{zz}^{nrel}	n_{zz}^{frel}	$n_{exp.}$
1.96	2.52	2.47	2.38	2.33	2.192
2.54	2.59	2.53	2.43	2.38	2.208